Published in final edited form as:

Nat Phys. 2020 ; 16(3): 346–350. doi:10.1038/s41567-019-0736-9.

Sixfold enhancement of superconductivity in a tunable electronic nematic system

Chris Eckberg[1,*], **Daniel J. Campbell**[1], **Tristin Metz**[1], **John Collini**[1], **Halyna Hodovanets**[1], **Tyler Drye**[1], **Peter Zavalij**[2], **Morten H. Christensen**[3], **Rafael M. Fernandes**[3], **Sangjun Lee**[4], **Peter Abbamonte**[4], **Jeffrey W. Lynn**[5], **Johnpierre Paglione**[1,6,*]

[1]Maryland Quantum Materials Center, Department of Physics, University of Maryland, College Park, MD, USA.

[2]Department of Chemistry, University of Maryland, College Park, MD, USA.

[3]School of Physics and Astronomy, University of Minnesota, Minneapolis, MN, USA.

[4]Department of Physics, Seitz Materials Research Laboratory, University of Illinois at Urbana-Champaign, Urbana, IL, USA.

[5]NIST Center for Neutron Research, National Institute of Standards and Technology, Gaithersburg, MD, USA.

[6]The Canadian Institute for Advanced Research, Toronto, Ontario, Canada.

Abstract

The electronic nematic phase—in which electronic degrees of freedom lower the crystal rotational symmetry—is commonly observed in high-temperature superconductors. However, understanding the role of nematicity and nematic fluctuations in Cooper pairing is often made more complicated by the coexistence of other orders, particularly long-range magnetic order. Here we report the enhancement of superconductivity in a model electronic nematic system that is not magnetic, and show that the enhancement is directly born out of strong nematic fluctuations associated with a quantum phase transition. We present measurements of the resistance as a function of strain in $Ba_{1-x}Sr_xNi_2As_2$ to show that strontium substitution promotes an electronically driven nematic order in this system. In addition, the complete suppression of that order to absolute zero temperature leads to an enhancement of the pairing strength, as evidenced by a sixfold increase in

[*]**Correspondence and requests for materials** should be addressed to C.E. or J.P. eckbergc@umd.edu; paglione@umd.edu.

Author contributions

C.E. and J.P. conceived and designed the experiments. C.E., D.J.C., T.M., H.H. and T.D. synthesized crystals and performed basic physical characterization. C.E. performed elastoresistivity measurements. J.C., S.L. and P.A. performed and analysed low-temperature X-ray characterization of the CDW phase. P.Z. performed and analysed 250 K single-crystal X-ray diffraction. J.L. performed preliminary neutron diffraction studies. M.H.C. and R.M.F. developed the phenomenological model describing the evolution of nematicity in this system. C.E., J.P., R.M.F. and M.H.C. wrote the manuscript with contributions from all authors.

Competing interests

The authors declare no competing interests.

Supplementary information is available for this paper at https://doi.org/10.1038/s41567-019-0736-9.

Peer review information *Nature Physics* thanks Dimitri Basov and the other, anonymous, reviewer(s) for their contribution to the peer review of this work.

the superconducting transition temperature. The direct relation between enhanced pairing and nematic fluctuations in this model system, as well as the interplay with a unidirectional charge-density-wave order comparable to that found in the cuprates, offers a means to investigate the role of nematicity in strengthening superconductivity.

High-temperature superconductivity in both cuprate[1,2] and iron-based materials[3-5] emerges from a notably complex normal state. Although magnetic spin fluctuations are commonly believed to drive Cooper pairing in both of these families, the common occurrence of a rotational symmetry-breaking nematic phase has captured increasing attention in recent years[6,7]. In contrast to a conventional structural transition, overwhelming evidence suggests that the nematic phase in these compounds is promoted by an electronic instability rather than lattice softening[8,9].

Theoretical analyses have shown that fluctuations associated with such an electronic nematic phase, particularly near a putative quantum critical point, can enhance superconductivity[10-14]. Nematic fluctuations are peaked at zero wavevector, and so favour pairing instabilities in several symmetry channels, in contrast to the case of magnetic fluctuations. Experiments have indeed shown a striking enhancement of nematic fluctuations centred at optimal tuning of superconductivity in a number of iron-based superconductors[8,9], and a strong tendency towards nematicity in high-critical temperature (T_c) cuprate materials[15-17]. However, the overarching presence of magnetic fluctuations emanating from proximate antiferromagnetic instabilities complicates our understanding of the relation between enhanced pairing and nematicity in most nematic materials. The $FeSe_{1-x}S_x$ substitution series is one exception, where the system exhibits both superconductivity and nematicity in the absence of magnetic order[18]. However, in this series, the superconducting transition temperature T_c is virtually unaffected by tuning through the nematic quantum critical point[18,19], leaving open questions about the influence of nematic fluctuations.

Here we present the discovery of electronic nematicity and evidence for nematic-fluctuation-enhanced superconductivity in $Ba_{1-x}Sr_xNi_2As_2$, a seemingly conventional nickel-based superconductor series that is readily tunable by chemical substitution and is void of magnetic order. $BaNi_2As_2$, the nickel-based analogue of the iron-based parent compound $BaFe_2As_2$, is a metallic compound that exhibits a strongly first-order structural transition from tetragonal to triclinic crystal structure at T_S = 135 K on cooling. Theoretical consideration has suggested that this structural distortion may originate from a predisposition to orbital ordering[20], and magnetic order has not been found in either the high- or low-temperature phase of $BaNi_2As_2$ to date[21-23]. Additionally, recent X-ray diffraction measurements have provided evidence for a previously unobserved unidirectional and incommensurate charge-density-wave (I-CDW) order that onsets at temperatures slightly above T_S (ref. [24]), followed by an abrupt transition to a new, commensurate CDW (C-CDW) order on cooling into the triclinic phase[24], hinting at a possible relationship between charge order and the structural distortion. In contrast, $SrNi_2As_2$ is tetragonal at all temperatures, and is not reported to exhibit CDW or magnetic order[25]. Both materials superconduct near 0.6 K, and thermodynamic experiments as well as first-principle analysis have indicated that superconductivity is of conventional origin in both materials[26,27]. In this

work, we study the superconducting phase and normal state properties of substituted $Ba_{1-x}Sr_xNi_2As_2$ crystals as a function of Ba/Sr content, finding that superconductivity is not only robust but is also dramatically enhanced when electronic nematic fluctuations are maximized at a quantum phase transition.

We begin by presenting the global phase diagram of the $Ba_{1-x}Sr_xNi_2As_2$ system in Fig. 1a. Replacing Ba with Sr suppresses the first-order tetragonal–triclinic structural distortion, as well as the simultaneous C-CDW order, in a continuous manner. On increasing x beyond the critical value $x_c = 0.7$, an abrupt 0 K tetragonal–triclinic structural phase transition is observed, and the system remains tetragonal and void of charge order in all samples between x_c and $x = 1$. The I-CDW phase, which appears at temperatures above T_S in pristine $BaNi_2As_2$, is also suppressed with increasing x until it merges with T_S and disappears altogether (upright red triangles in Fig. 1a). Additionally, the coherence length of the I-CDW, estimated from the full-width at half-maximum of its associated X-ray peaks, is reduced from over 1,000 Å to only several hundred ångströms with increasing x between $x = 0$ and $x = 0.4$, and the structure vanishes in samples with larger x. For instance, at $x = 0.65$ the system transitions from a tetragonal structure with no incommensurate charge-order superstructure peaks into a triclinic structure with a C-CDW superstructure at 50 K.

In parallel, superconductivity in $Ba_{1-x}Sr_xNi_2As_2$ single crystals changes across the phase diagram (Fig. 1b). Approaching x_c from the $BaNi_2As_2$ endmember, resistive and magnetic signatures of T_c appear to climb in temperature at concentrations above $x = 0.5$. However, despite the onset of zero resistance at increasing temperature, the 'bulk' signature of T_c, as determined by specific heat measurements (see Supplementary Fig. 6), remains relatively unchanged for $x < x_c$. On crossing the zero-temperature structural phase boundary, an abrupt enhancement in bulk T_c is observed from approximately 0.5 K in $x = 0.68$ samples to near 3.5 K at $x = 0.71$. Optimally substituted $x = 0.71$ presents a very robust superconducting transition as measured by resistivity, diamagnetism and specific heat anomaly, well fitted by a single-band model with a BCS gap (Fig. 2 inset). Remarkably, this optimal T_c of 3.5 K at $x = 0.71$ marks a nearly sixfold enhancement compared to either of the Sr- or Ba-based endmembers. The superconducting transition then decreases continuously with increasing x towards that of $SrNi_2As_2$. This change in pairing strength occurs through a regime with no notable change in structure, and virtually unchanged Sommerfeld coefficients of approximately 10 mJ mol^{-1} K^{-2} (Fig. 2), indicating that the T_c enhancement cannot be explained by changes in the electronic density of states.

Consistent with prior studies[28-30], the $Ba_{1-x}Sr_xNi_2As_2$ system exhibits a discontinuity in the Debye temperature Θ_D at x_c. However, Θ_D remains approximately constant between $x = 0.71$ ($\Theta_D = 198$ K) and $x = 0.86$ ($\Theta_D = 188$ K), despite a nearly twofold difference in the superconducting T_c. This contrast indicates that, like the electronic density of states, changes in lattice stiffness do not capture the enhancement in the pairing potential. Rather, the smooth increase in critical temperature on approaching x_c from above is reminiscent of a fluctuation-driven superconducting enhancement. Given the very abrupt first-order nature of the triclinic–tetragonal structural boundary, which appears to drop at x_c, an increase in pairing strength must arise from a hitherto hidden coupling to the electronic system that can enhance pairing.

Having ruled out the usual sources of a T_c increase expected for a conventional phonon-mediated superconductor (density of states and Debye frequency), we propose that this enhancement is driven by the presence of nematic fluctuations. Indeed, the existence of a tetragonal-to-triclinic transition shows that rotational symmetry is broken in this system. To investigate whether this transition is driven by electronic, rather than lattice degrees of freedom, we perform elastoresistance measurements. The elastoresistance tensor $m_{ij,kl} = \frac{\partial(\Delta\rho/\rho)_{ij}}{\partial\epsilon_{kl}}$ corresponds to the rate of change of the normalized resistivity $(\Delta\rho/\rho)_{ij}$ on application of external strain ϵ_{kl}. As discussed in ref.[8], when the applied strain transforms as one of the non-trivial irreducible representations Γ_μ of the point group, $\epsilon_{kl} \equiv \varepsilon_\mu$, the resistivity change in that channel is proportional to the corresponding nematic order Ψ_μ, $(\Delta\rho/\rho)_{ij} \propto \Psi_\mu$. As ε_μ acts as a conjugate field to the nematic order parameter Θ_μ, the corresponding elastoresistance m_{Γ_μ} becomes proportional to the bare nematic susceptibility without renormalization by the lattice degrees of freedom:

$$m_{\Gamma_\mu} \propto \chi^{\mu}_{\mathrm{nem}} \equiv \frac{\partial\psi_\mu}{\partial\varepsilon_\mu} \quad (1)$$

The key point is that, if m_{Γ_μ} shows a diverging behaviour above the rotational symmetry-breaking transition, it implies that the latter is driven by electronic degrees of freedom. If m_{Γ_μ} shows instead a weak temperature dependence, it implies that the transition is a standard lattice-driven structural transition.

In the case of tetragonal $Ba_{1-x}Sr_xNi_2As_2$, there are three symmetry-distinct channels of rotational symmetry-breaking, corresponding to the three irreducible representations B_{1g}, B_{2g} and E_g of the point group D_{4h}. In terms of charge degrees of freedom, they correspond to quadrupolar charge order with form factors $x^2 - y^2$, xy and (xz, yz), respectively. In terms of lattice degrees of freedom, the first two correspond to orthorhombic distortions $\varepsilon_{B_{1g}}$ and $\varepsilon_{B_{2g}}$, and the third, to a monoclinic distortion $(\varepsilon^1_{E_g}, \varepsilon^2_{E_g})$ of the tetragonal lattice. Importantly, in the triclinic phase of $Ba_{1-x}Sr_xNi_2As_2$, all four lattice distortions are present. This indicates the potential that one or more of the three nematic susceptibilities $\chi^{B_{1g}}_{\mathrm{nem}}$, $\chi^{B_{2g}}_{\mathrm{nem}}$ and $\chi^{E_g}_{\mathrm{nem}}$ may be diverging above T_S.

To measure the nematic susceptibilities, we use a piezoelectric elastoresistance technique (see Methods), applying in situ tunable biaxial strain to $Ba_{1-x}Sr_xNi_2As_2$ single-crystal specimens. Figure 3 presents the elastoresistance $m_{12} - m_{11}$, which is proportional to $\chi^{B_{1g}}_{\mathrm{nem}}$, in stoichiometric $BaNi_2As_2$. While $m_{12} - m_{11}$ is negative at temperatures well above the structural transition, it becomes positive near $T_S \approx 135$K (Fig. 3a,b). Before it peaks at T_S, however, $m_{12} - m_{11}$ starts displaying strain-hysteretic behaviour at a temperature of about 148 K (blue symbols in Fig. 3c). While $m_{12} - m_{11}$ is still presented in the temperature range of strain-hysteretic resistance in Fig. 3c, $T < 148$ K, it is important to note that these values are no longer true nematic susceptibilities, since true nematic susceptibility is well defined only in the regime of linear response. Crucially, the onset of strain-hysteresis in the

elastoresistivity experiment coincides with the emergence of I-CDW peaks (red symbols in Fig. 3c), which appear at approximately 150 K. Bragg reflections corresponding to this structure are observed at wavevector (0.28 0 0) while no peaks are observed in the orthogonal (0 0.28 0) direction, indicating that the superstructure does not possess C_4 symmetry. The simultaneous observation of unidirectional CDW peaks and strain-hysteretic $m_{12} - m_{11}$ transport in $BaNi_2As_2$ indicates tetragonal symmetry-breaking in the B_{1g} channel at a temperature $T_N \approx 150$ K that is higher than T_S. However, the electronic nematic susceptibility proportional to $m_{12} - m_{11}$ does not seem to diverge near T_N—in fact, it is nearly temperature-independent above T_N. This is indicative that the transition is driven primarily not by electronic, but by lattice degrees of freedom.

The evolution of the elastoresistivity in the B_{1g} channel in substituted $Ba_{1-x}Sr_xNi_2As_2$ crystals is presented in Fig. 4. First, we note that the onset of strain-hysteretic behaviour at T_N, indicated by the light-grey shaded areas in the plots, moves closer to the triclinic structural transition T_S, and eventually merges with the latter for $x = 0.63$. Second, the modest temperature dependence of $m_{12} - m_{11}$ above T_N in stoichiometric $BaNi_2As_2$ is not reflected in more heavily substituted samples. Indeed, $m_{12} - m_{11}$ starts displaying a diverging behaviour above T_N over a wide temperature range in $Ba_{1-x}Sr_xNi_2As_2$ samples with increasing x. These data may be reasonably fitted to a modified Curie–Weiss function ($\chi_{nem}^{B_{1g}} = \frac{\lambda}{a_0(T - T_N)} + \chi_0$) above T_N, indicating diverging susceptibilities reminiscent of electronically driven nematic order. Therefore, our elastoresistance data show a change in the character of the tetragonal symmetry-breaking transition from lattice-driven for small x to electronically driven for x near optimal substitution. This is corroborated by a phenomenological Ginzburg–Landau calculation to model the nematic susceptibility data (see Supplementary Section I).

While the B_{1g} nematic susceptibility diverges, the B_{2g} susceptibility is only very weakly temperature dependent in samples with $x = 0$ and $x = 0.63$ (see Supplementary Figs. 10 and 11). The absence of a diverging B_{2g} susceptibility indicates that the strengthening of the electronic nematic fluctuations is limited to the B_{1g} symmetry channel, despite the presence of B_{2g} symmetric rotational symmetry-breaking at the triclinic structural transition. This indicates that the triclinic phase transition cannot be attributed solely to electronic degrees of freedom, and contrasts with the structurally related Fe-based superconductors, where ubiquitous signatures of nematicity in the B_{2g} channel are reported[9].

The diverging B_{1g} susceptibility persists in the $x = 0.75$ samples, which feature no discernible phase transition in thermal, magnetic, transport or diffraction measurements down to the lowest temperatures. Despite the absence of any evident phase transition, $m_{12} - m_{11}$ data for $Ba_{0.25}Sr_{0.75}Ni_2As_2$ exhibit a clear peak and subsequent downturn at 25 K. Such a nematic susceptibility peak, in the absence of any apparent order (see Supplementary Fig. 12), is unprecedented in its observation. In analogy to more familiar magnetic systems, it may be an indication of a freezing nematic glass, or possibly an artefact of quenched disorder subverting long-range nematic correlations.

Returning to the overall phase diagram of $Ba_{1-x}Sr_xNi_2As_2$, the amplitude of the B_{1g} nematic susceptibility is overlaid with the triclinic and CDW phase boundaries in Fig. 1. Owing to our inability to extract a nematic susceptibility in the triclinic phase, as well as the uncertainty in the superconducting T_c in undersubstituted samples, we focus our analysis on crystals that are tetragonal to lowest temperatures. Approaching x_c from the $SrNi_2As_2$ endmember, a smooth enhancement of electronic nematic fluctuations is observed at the lowest temperatures. In contrast to the stagnant behaviour of other thermodynamic quantities, such as specific heat, nematic fluctuations grow concurrently with the enhancing superconducting T_c, with an over tenfold enhancement of $m_{12} - m_{11}$ from $x = 1$ to x_c. It is through the exchange of these excitations that the superconducting enhancement in the tetragonal phase can be explained[11,13,14]. The strength of this enhancement, corresponding to a nearly sixfold increase in T_c from the series endmembers, establishes nematic fluctuations as a promising mechanism for enhancing Cooper pairing, even in a conventional superconductor such as, presumably, the one studied here.

The origin of the nematic order in $Ba_{1-x}Sr_xN_2As_2$ cannot be inferred solely from elastoresistance measurements. In the structurally and chemically similar $BaFe_2As_2$ compounds, the B_{2g} electronic nematic order is proposed to be driven by magnetic degrees of freedom, since the stripe magnetic ground state breaks the tetragonal symmetry in the same channel[31-33]. The $Ba_{1-x}Sr_xNi_2As_2$ series, in contrast, exhibits B_{1g} symmetric nematic fluctuations and no known magnetic order. It does exhibit, however, unidirectional CDW order that breaks tetragonal symmetry in the B_{1g} channel. It is therefore tempting to attribute the nematic instability in $Ba_{1-x}Sr_xNi_2As_2$ as driven by charge fluctuations. Indeed, comparing in Fig. 3c the square of the CDW X-ray peak intensity to the width of the elastoresistance hysteresis, which is a proxy of the nematic order parameter (see Supplementary Section I), we observe a nearly linear relationship between the two quantities, as expected by symmetry considerations. This lends further support to the assumption of charge-driven nematicity, although, as the origins of and relationship between I-CDW and C-CDW phases has not been determined yet, it is impossible to conclude if one of the two present charge orders is predominantly associated with the underlying nematicity. Ultimately, these observations provide a compelling scenario to explain the phase diagram of $Ba_{1-x}Sr_xNi_2As_2$ in terms of two cooperative ordered states: a charge-driven electronic nematic phase and a lattice-driven triclinic phase. While both break the tetragonal symmetry in the B_{1g} channel, the latter also breaks additional symmetries that our elastoresistance measurements show cannot be accounted for solely by electronic degrees of freedom (as evidenced by the lack of divergence of the B_{2g} nematic susceptibility).

The likely relationship between nematic and CDW order evokes comparison to the cuprate superconductors, where short-range, unidirectional I-CDW stripe order and electronic anisotropies were reported in the pseudogap phase[7,16,34]. In the cuprates, it was proposed that the microscopic tendency is towards unidirectional CDW order, with long-range coherence being precluded by quenched disorder[35]. The nematic phase is more robust to disorder, however, surviving as a vestige of the suppressed stripes. In $Ba_{1-x}Sr_xNi_2As_2$, unlike the cuprate compounds, long-range CDW superstructures survive for sufficiently small x.

Online content

Any methods, additional references, Nature Research reporting summaries, source data, extended data, supplementary information, acknowledgements, peer review information; details of author contributions and competing interests; and statements of data and code availability are available at https://doi.org/10.1038/s41567-019-0736-9.

Methods

Crystal synthesis.

$Ba_{1-x}Sr_xNi_2As_2$ single crystals were synthesized using pre-reacted NiAs self-flux combined with Ba and Sr pieces in a 4:1–x:x ratio as previously reported[22]. Materials were heated to 1,180 °C before being slowly cooled to 980 °C at 2 °C h^{-1}. At this point, the furnace was turned off and allowed to cool to room temperature naturally. Once cool, crystals with typical dimensions of 2 mm × 2 mm × 0.5 mm were mechanically extracted from flux. The chemical compositions of the resulting crystals were determined using a combination of energy-dispersive spectroscopy and single-crystal X-ray refinements.

Transport, specific heat and magnetization.

Transport and heat capacity data were taken using both a Quantum Design Physical Property Measurement System and a Quantum Design DynaCool. Heat capacity data were generally collected via a relaxation method. To observe the first-order phase transition on both warming and cooling, select heat capacity measurements were modified to be sensitive to both transitions. Within these modified measurements, an extended heat pulse was applied and heat capacity was extracted using a local derivative approach. D.c.-magnetization measurements were taken using a SQUID-VSM option in a Quantum Design MPMS3 system. A home-made coil[37] was also used in a Quantum Design adiabatic demagnetization refrigerator insert to measure a.c. susceptibility down to 0.1 K.

X-ray diffraction.

The 250 K structural data were collected on single crystals in a Bruker APEX-II CCD system equipped with a graphite monochromator and a MoKα sealed tube (λ = 0.71073 Å), and were refined using the Bruker SHELXTL Software Package. Temperature-dependent diffraction measurements were carried out using a Xenocs GeniX 3D MoKα microspot X-ray source with multilayer focusing optics and a Mar345 image plate detector. Single-crystal samples were cooled with a closed-cycle cyrostat and mounted to a Huber four-circle diffractometer.

Elastoresistivity.

To measure the nematic susceptibilities, we used the piezoelectric elastoresistance technique of refs. [8,38]. Within the D_{4h} point group, elastoresistive coefficients $m_{12} - m_{11}$ are directly proportional to $\chi_{nem}^{B_{1g}}$ while m_{66} is directly proportional to $\chi_{nem}^{B_{2g}}$ (ref.[39]). Both $m_{12} - m_{11}$ and m_{66} were measured in samples adhered directly to a lead zirconium titanate piezoelectric stack using a strain-transmitting epoxy as discussed in refs. [8,38]. By applying a voltage to the

stack, variable bi-axial strain was applied in situ. The magnitude of the applied strain was measured using a strain gauge mounted on the reverse side of the stack. The strain was measured along a single piezo axis (ε_{xx} in the convention used within this text), and orthogonal strain was calculated using the known Poisson's ratio of the stack. $m_{12} - m_{11}$ elastoresistive coefficients were measured using two samples mounted in a mutual orthogonal geometry, with the crystal (1 0 0) axis mounted parallel and perpendicular to the piezo poling direction. For all measurements requiring two samples, a single crystal was polished to a suitable thickness (≤60 μm) and then cleaved into two pieces. These two pieces were used for a single measurement to ensure consistent physical properties across the two orthogonal samples. m_{66} data were collected using a single sample wired in a transverse geometry. Strain was then applied along the crystallographic (1 1 0) direction[38]. Crystal geometry (specifically a narrow c-axis cross-section and tendency towards cleaving along the crystallographic (1 0 0) direction) made m_{44}, $\chi_{\mathrm{nem}}^{\mathrm{E_g}}$, experimentally inaccessible.

Supplementary Material

Refer to Web version on PubMed Central for supplementary material.

Acknowledgements

Research at the University of Maryland was supported by the AFOSR Grant No. FA9550-14-10332, the National Science Foundation Grant No. DMR1905891, and the Gordon and Betty Moore Foundation's EPiQS Initiative through Grant No. GBMF4419. We also acknowledge support from the Maryland Quantum Materials Center as well as the Maryland Nanocenter and its FabLab. The identification of any commercial product or trade name does not imply endorsement or recommendation by the National Institute of Standards and Technology. Theory work (R.M.F. and M.H.C.) was supported by the US Department of Energy, Office of Science, Basic Energy Sciences under award number DE-SC0012336. X-ray experiments at UIUC were supported by DOE grant DE-FG02-06ER46285. P.A. acknowledges support from the Gordon and Betty Moore Foundation's EPiQS initiative through grant GBMF4542.

Data availability

Source data for Figs. 1-4 are provided with the paper. All other data that support the plots within this paper and other findings of this study are available from the corresponding author upon reasonable request.

References

1. Orenstein J & Millis AJ Advances in the physics of high-temperature superconductivity. Science 288, 468–474 (2000). [PubMed: 10775099]
2. Keimer B, Kivelson SA, Norman MR, Uchida S & Zaanen J From quantum matter to high-temperature superconductivity in copper oxides. Nature 518, 179–186 (2015). [PubMed: 25673411]
3. Paglione J & Greene R High-temperature superconductivity in iron-based materials. Nat. Phys 6, 645–658 (2010).
4. Johnston DC The puzzle of high temperature superconductivity in layered iron pnictides and chalcogenides. Adv. Phys 59, 803–1061 (2010).
5. Stewart GR Superconductivity in iron compounds. Rev. Mod. Phys 83, 1589–1652 (2011).
6. Fernandes RM, Chubukov AV & Schmalian J What drives nematic order in iron-based superconductors? Nat. Phys 10, 97–104 (2014).
7. Kivelson S, Fradkin E & Emery V Electronic liquid crystal phases of a doped Mott insulator. Nature 393, 550–553 (1998).

8. Chu J-H, Kuo H-H, Analytis JG & Fisher IR Divergent nematic susceptibility in an iron arsenide superconductor. Science 337, 710–712 (2012). [PubMed: 22879513]
9. Kuo H-H, Chu J-H, Palmstrom JC, Kivelson SA & Fisher IR Ubiquitous signatures of nematic quantum criticality in optimally doped Fe-based superconductors. Science 352, 958–962 (2016). [PubMed: 27199422]
10. Metlitski MA, Mross DF, Sachdev S & Senthil T Cooper pairing in non-Fermi liquids. Phys. Rev. B 91, 115111 (2015).
11. Lederer S, Schattner Y, Berg E & Kivelson SA Enhancement of superconductivity near a nematic quantum critical point. Phys. Rev. Lett 114, 097001 (2015). [PubMed: 25793842]
12. Lederer S, Schattner Y, Berg E & Kivelson SA Superconductivity and non-Fermi liquid behavior near a nematic quantum critical point. Proc. Natl Acad. Sci. USA 114, 4905–4910 (2017). [PubMed: 28439023]
13. Kang J & Fernandes RM Superconductivity in FeSe thin films driven by the interplay between nematic fluctuations and spin–orbit coupling. Phys. Rev. Lett 117, 217003 (2016). [PubMed: 27911515]
14. Klein A, Wu Y & Chubukov AV Multiple intertwined pairing states and temperature-sensitive gap anisotropy for superconductivity at a nematic quantum-critical point. npj Quantum Mater. 4, 55 (2019).
15. Hinkov V et al. Electronic liquid crystal state in the high-temperature superconductor $YBa_2Cu_2O_2$. Science 319, 597–600 (2008). [PubMed: 18187621]
16. Vojta M Lattice symmetry breaking in cuprate superconductors: stripes, nematics, and superconductivity. Adv. Phys 58, 699–820 (2009).
17. Sato Y et al. Thermodynamic evidence for a nematic phase transition at the onset of the pseudogap in $YBa_2Cu_2O_2$. Nat. Phys 13, 1074–1078 (2017).
18. Hosoi S et al. Nematic quantum critical point without magnetism in $FeSe_{1-x}S_{1-x}$ superconductor. Proc. Natl Acad. Sci. USA 113, 8139–8143 (2016). [PubMed: 27382157]
19. Reiss P et al. Suppression of electronic correlations by chemical pressure from FeSe to FeS. Phys. Rev. B 96, 121103 (2017).
20. Yamakawa Y, Onari S & Kontani H Zigzag chain structure transition and orbital fluctuations in Ni-based superconductors. J. Phys. Soc. Jpn 82, 094704 (2013).
21. Ronning F et al. The first order phase transition and superconductivity in $BaNi_2As_2$ single crystals. J. Phys. Condens. Matter 20, 342203 (2008).
22. Sefat AS et al. Structure and anisotropic properties of $BaFe_{2-x}Ni_{2-x}As_{2-x}$ (x = 0, 1, and 2) single crystals. Phys. Rev. B 79, 094508 (2009).
23. Kothapalli K, Ronning F, Bauer ED, Schultz AJ & Nakotte H Single-crystal neutron diffraction studies on Ni-based metal-pnictide superconductor $BaNi_2s_2$. J. Phys. Conf. Ser 251, 012010 (2010).
24. Lee S et al. Unconventional charge density wave order in the pnictide superconductor $B(Ni_{1-x}Co_{1-x})_{1-x}As_{1-x}$. Phys. Rev. Lett 122, 147601 (2019). [PubMed: 31050473]
25. Bauer ED, Ronning F, Scott BL & Thompson JD Superconductivity in $SrNi_2As_2$ single crystals. Phys. Rev. B 78, 172504 (2008).
26. Subedi A & Singh DJ Density functional study of $BaNi_2As_2$: electronic structure, phonons, and electron–phonon superconductivity. Phys. Rev. B 78, 132511 (2008).
27. Kurita N et al. Low-temperature magnetothermal transport investigation of a Ni-based superconductor $BaNi_2As_2$: evidence for fully gapped superconductivity. Phys. Rev. Lett 102, 147004 (2009). [PubMed: 19392475]
28. Kudo K, Takasuga M, Okamoto Y, Hiroi Z & Nohara M Giant phonon softening and enhancement of superconductivity by phosphorus doping of $BaNi_2As_2$. Phys. Rev. Lett 109, 097002 (2012). [PubMed: 23002873]
29. Kudo K, Takasuga M & Nohara M Copper doping of $BaNi_2As_2$: giant phonon softening and superconductivity enhancement. Preprint at http://arXiv.org/abs/1704.04854 (2017).
30. Eckberg C et al. Evolution of structure and superconductivity in $Ba(Ni_{1-x}Co_{1-x})_{1-x}As_{1-x}$. Phys. Rev. B 97, 224505 (2018).

31. Cano A, Civelli M, Eremin I & Paul I Interplay of magnetic and structural transitions in iron-based pnictide superconductors. Phys. Rev. B 82, 020408 (2010).
32. Fernandes RM, Chubukov AV, Knolle J, Eremin I & Schmalian J Preemptive nematic order, pseudogap, and orbital order in the iron pnictides. Phys. Rev. B 85, 024534 (2012).
33. Fernandes RM, Böhmer AE, Meingast C & Schmalian J Scaling between magnetic and lattice fluctuations in iron pnictide superconductors. Phys. Rev. Lett 111, 137001 (2013). [PubMed: 24116808]
34. Achkar AJ et al. Nematicity in stripe-ordered cuprates probed via resonant x-ray scattering. Science 351, 576–578 (2016). [PubMed: 26912696]
35. Nie L, Tarjus G & Kivelson SA Quenched disorder and vestigial nematicity in the pseudogap regime of the cuprates. Proc. Natl Acad. Sci. USA 111, 7980–7985 (2014). [PubMed: 24799709]
36. Johnston DC Elaboration of the α-model derived from the BCS theory of superconductivity. Supercond. Sci. Technol 26, 115011 (2013).
37. Yonezawa S, Higuchi T, Sugimoto Y, Sow C & Maeno Y Compact AC susceptometer for fast sample characterization down to 0.1 K. Rev. Sci. Instrum 86, 093903 (2015). [PubMed: 26429453]
38. Shapiro MC, Hristov AT, Palmstrom JC, Chu J-H & Fisher IR Measurement of the $B1_g$ and B_{2g} components of the elastoresistivity tensor for tetragonal materials via transverse resistivity configurations. Rev. Sci. Instrum 87, 063902 (2016). [PubMed: 27370465]
39. Shapiro MC, Hlobil P, Hristov AT, Maharaj AV & Fisher IR Symmetry constraints on the elastoresistivity tensor. Phys. Rev. B 92, 235147 (2015).

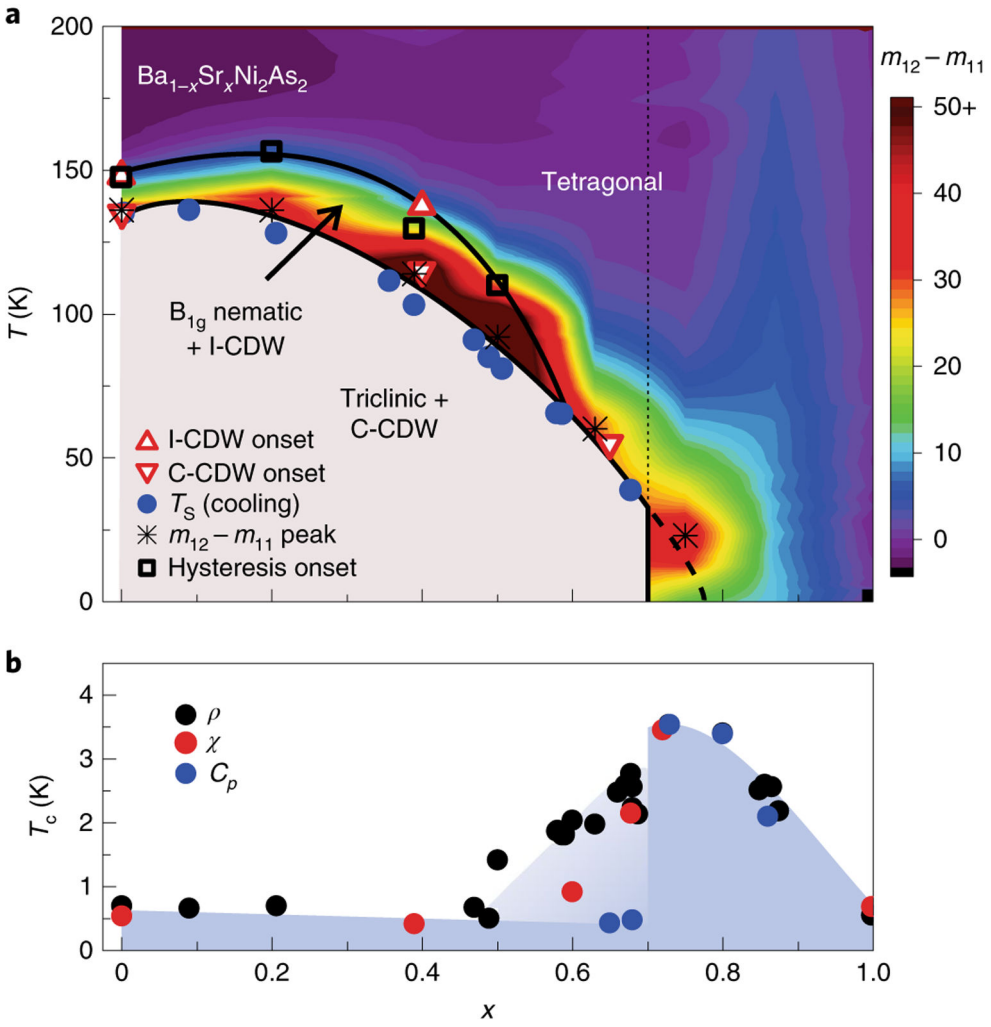

Fig. 1 | Evolution of structural, charge and nematic orders in $Ba_{1-x}Sr_xNi_2As_2$.
This system presents an interplay of structural, charge and nematic instabilities that evolve as a function of chemical pressure induced by Sr substitution. It features an enhancement of the superconducting transition temperature in the region where charge and nematic orders cease to be long range, and nematic fluctuations are peaked at the lowest temperatures. **a**, Single-crystal measurements form a phase diagram consisting of onsets of I-CDW order (upright red triangles), elastoresistive strain-hysteresis (open black squares), C-CDW order (inverted red triangles), and the cooling transition of the first-order triclinic structural distortion (filled blue circles). The black asterisks mark the peak position of nematic susceptibilities, which extend beyond the disappearance (vertical dashed line) of the triclinic phase at $x_c = 0.70$. The overlaid colour scale represents interpolated values of the nematic susceptibility $m_{12} - m_{11}$ generated from data taken in $Ba_{1-x}Sr_xNi_2As_2$ single crystals with $x = 0$, 0.2, 0.4, 0.5, 0.63, 0.75, 0.87 and 1.0. **b**, Superconducting transition temperatures T_c in $Ba_{1-x}Sr_xNi_2As_2$ single crystals determined by transport (black circles), magnetization (red circles) and heat capacity (blue circles) measurements. The dark blue shading reflects the true, bulk T_c (as confirmed via heat capacity transitions) while the light blue region indicates

filamentary superconductivity observed as broad transitions in transport and magnetic measurements, but absent in heat capacity.

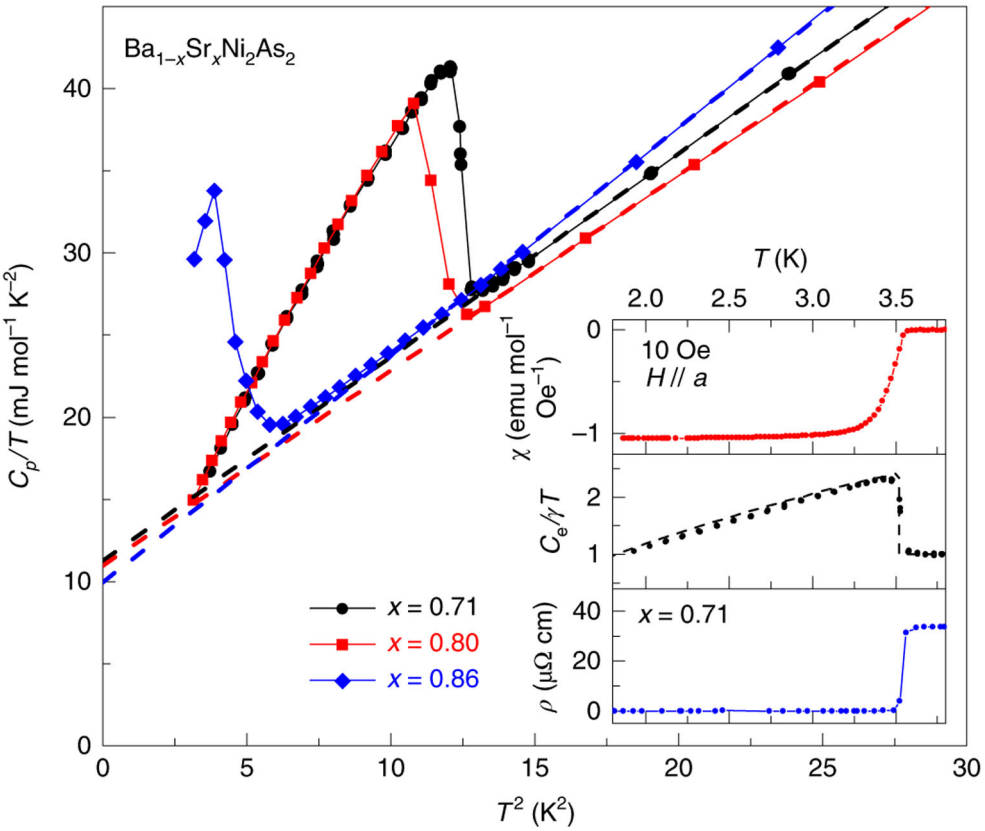

Fig. 2 | Enhancement of superconducting transition temperature.
Heat capacity measurements in slightly over-substituted $Ba_{1-x}Sr_xNi_2As_2$ single crystals with $x = 0.71$, 0.80 and 0.86 depict dramatic enhancement of T_c. This contrasts with the very small changes in Sr concentrations, Debye temperatures (as determined by the T^3 phonon contribution shown by the dashed lines) and density of states (as determined by Sommerfeld coefficients, given by the extrapolation of the dashed lines to $T = 0$) across these samples. Inset: the superconducting transition in the same $x = 0.71$ single-crystal specimen, measured by field-cooled magnetization (upper panel), electronic heat capacity (centre panel) and transport (lower panel), is consistent with an enhanced T_c of 3.5 K, larger than the values at either series endmember. The dashed line in the heat capacity data indicates the predicted electronic heat capacity anomaly for a single-band, s-wave superconductor, with a BCS gap[36].

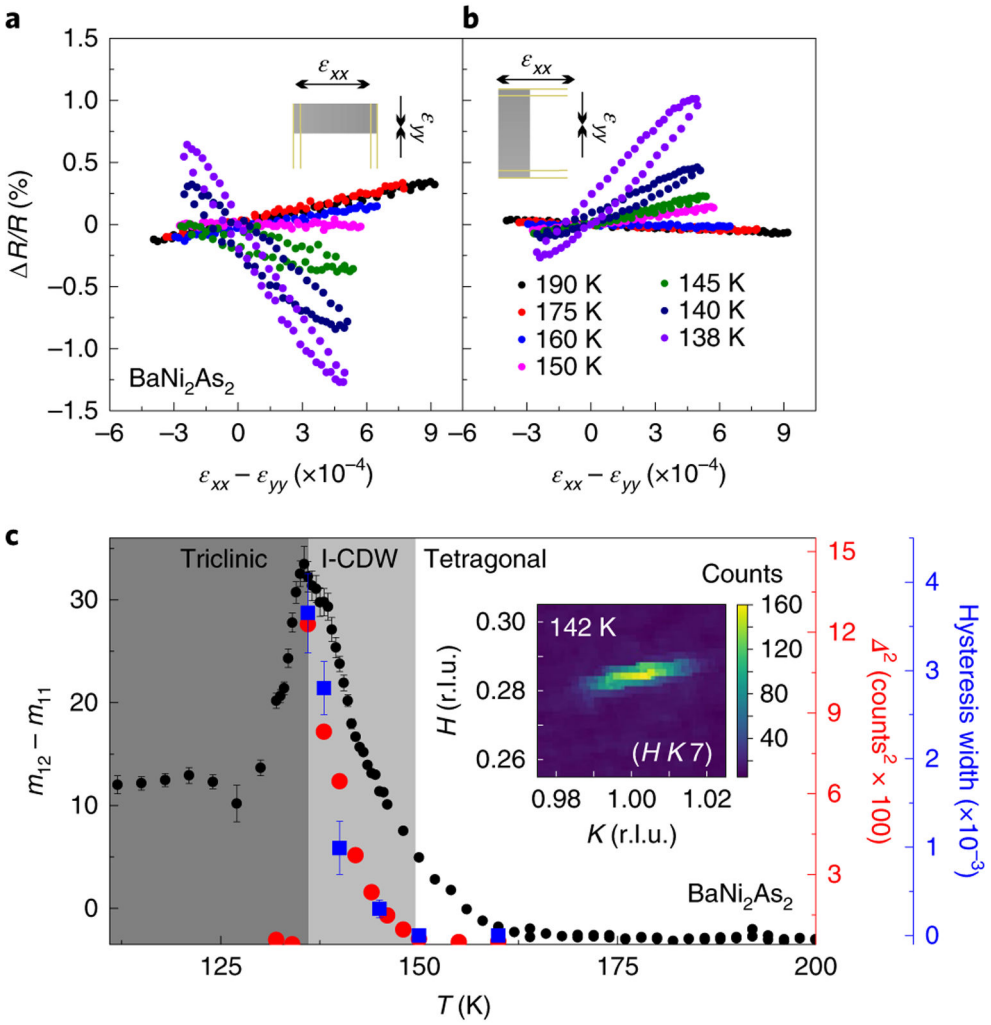

Fig. 3 | Electronic nematic and charge orders in $BaNi_2As_2$.

a,**b**, A divergent B_{1g} nematic susceptibility, determined by elastoresistivity measurements shown in the strain-dependent resistance isotherms for single crystals mounted parallel (**a**) and perpendicular (**b**) to the poling direction of the piezo stack, is comparable in magnitude to that of $BaFe_2As_2$ (ref.[8]) and is accompanied by two notable ordered states. **c**, The nematic susceptibility in the B_{1g} channel, proportional to the elastoresistance $m_{12} - m_{11}$, is nearly flat at high temperatures before growing when approaching the I-CDW-ordered phase (light grey region), and then peaking at the structural transition into the triclinic phase (dark grey region). (Black symbols include error bars representing 90% confidence intervals of data.) Strain-hysteretic behaviour of the elastoresistance is observed to begin at the same temperature where I-CDW is seen. A comparison of the squared peak intensity of a (0.28 0 0) I-CDW superstructure reflection (the (−1.72 1 7) peak; red symbols) and the elastoresistive hysteresis width (blue symbols) shows a nearly linear relationship. Strain-dependent isotherms were repeated three times at each temperature, and hysteresis widths were measured at the widest point. The error bars represent extremal values of the hysteresis width between separate measurements. Inset: an (*H K*) map (in reciprocal lattice units, r.l.u.)

of the reciprocal space at 142 K, displaying a reflection from the superstructure at wavevector (0.28 1 7).

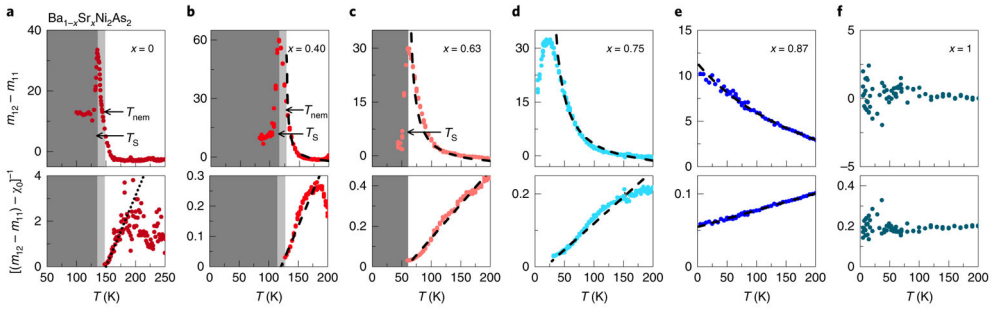

Fig. 4 | Nematic susceptibilities of $Ba_{1-x}Sr_xNi_2As_2$ single crystals.
a–f, The B_{1g} nematic susceptibility exhibits a continuous evolution with x, eventually disappearing in $SrNi_2As_2$ ($x = 1$), as shown in the top panels. The dark grey regions indicate triclinic structural phases in $x = 0$, 0.40 and 0.63, and light grey regions (only in $x = 0$ and 0.40) indicate temperatures where elastoresistive hysteresis is observed in the tetragonal structure. The lower panels display the inverse susceptibilities $[(m_{12} - m_{11}) - \chi_0]^{-1}$, truncated at the onset of nematic order. The constant, χ_0, is a temperature-independent component of the elastoresistance, coming from factors unrelated to nematic order, including changing sample geometry, and is determined through fitting data to the modified Curie–Weiss functional form; $m_{12} - m_{11} = \frac{\lambda}{a_0(T - T_{N0})} + \chi_0$. The bare nematic transition temperature T_{N0} extracted from such a fit may differ slightly from the observed nematic transition temperature due to coupling between the structural and electronic degrees of freedom. The black dashed lines show the results of this fitting. No fitting is presented in samples of $x = 0$ or $x = 1$, as neither of these show Curie–Weiss-like divergence. The dotted black line in the lower panel of **a** is a guide for the eye, indicating incipient nematic fluctuations in the vicinity of T_N. At $x = 0.75$, which exhibits no nematic, structural or charge-ordered transitions and remains tetragonal to the lowest temperatures, the nematic susceptibility exhibits a broad peak at 25 K.